Accurate Estimation of Wheel Pressure-Sinkage Traits on Sandy Terrain using In-Wheel Sensor System

Takayuki Shirai*, Genya Ishigami*

*Department of Mechanical Engineering, Keio University, Japan
e-mail: takayuki@z8.keio.jp, ishigami@mech.keio.ac.jp

Abstract

Planetary rovers need to possess high traversability on loose sand, but such terrain often impedes the rover traverse and also induces large wheel slip. Therefore, an accurate estimation of wheel-soil interaction characteristics is an important issue. Recent studies in the wheel-soil interaction mechanics have revealed that the classical wheel model can not properly address the wheel pressure distribution. In this work, an in-wheel sensor system is developed that equips two sensory devices on its wheel surface: the pressure sensors for direct measurement of the pressure distribution and the light sensors for wheel-soil contact angle estimation. This sensor configuration enables the simultaneous measurement of the pressure distribution as well as the wheel-soil contact angles while the wheel driving on loose sand. The in-wheel sensor therefore achieves to clarify a detailed relationship between the driving characteristics.

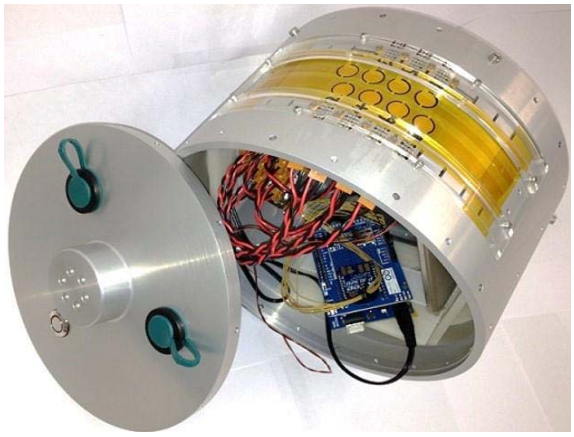

Figure 1. Advanced Sensor-wheel with Pressure and Light detection

1 Introduction

Planetary rovers are indispensable used as the robot that carry out tasks for recent space missions. The Mars Exploration Rover Mission or the Mars Science Laboratory Mission (NASA/JPL) are the most famous example. On the surface of the Mars or Moon, wheels of the rover may be in trouble with large slips and sinkages, since the planetary surfaces are covered with loose soil. In the MER mission, one of the rovers Spirit had got stuck in the sandy soil, resulting in the mission suspend. Therefore, an accurate estimation of the wheel-soil interaction mechanics is of an important issue.

In general, Terramechanics focuses on the machine-soil interaction, and has been widely used for the above mentioned problem. A wheel-soil interaction model based on the terramechanics was proposed by Bekker [1]. This model was expanded such that the model is applicable for various types of soils [2], and contributes to the behavior estimation of rovers running on the off-road [3][4].

This wheel-soil interaction model induces various soil parameters [5][6]. Also the classical model assumes homogeneous soil and flat terrain surface. However, the behavior of rovers in the real environment may often violate such the assumptions: the wheel slips or sinkage deforms the terrain condition. It is difficult to accurately estimate the actual phenomenon observed at the wheel surface such as slips and sinkages. Therefore, many studies have dedicated to verifying the wheel-soil interaction model [7][8]. In these studies, the classical interaction model was applied to calculate the pressure distribution generated at the wheel contact patch, contact angle, and sinkage.

Iagnemma et al. proposed an accurate measurement of the wheel characteristics based on the information obtained from wheel motors and cameras [9]. Associating the value of motor torque with that of sinkage obtained by cameras prepared at the outside of the wheel, wheel mobility on loose sand can be predicted. However, in this case, the motor torque measurement may not be stable owing to a dynamic wheel behavior, and the sinkage obtained by image processing may often have a critical error owing to the lighting conditions or image quality.

Nagatani et al. developed an in-wheel sensor, the surface of which is covered with several tactile pressure sensor arrays [10]. Each sensor directly measures the pressure value and determine the pressure distribution between wheel and soil. However, they remarked that the wheel sinkage (wheel-sand contact angles) cannot be accurately determined because of low signal-to-noise ratio of the pressure sensors. They also concluded that the

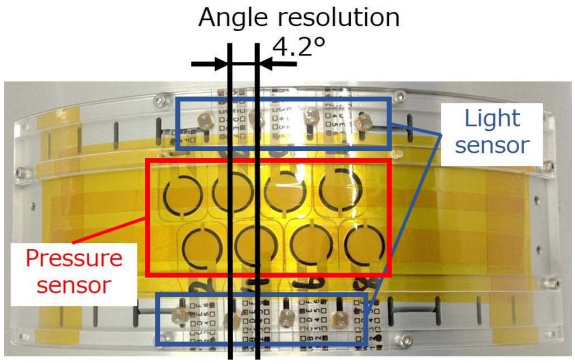

Figure 2. Sensing patch of ASPL

pressure distribution area measured by the in-wheel sensor may be considerably smaller than the real wheel-soil contact area.

In this work, an in-wheel sensor system called ASPL (Advanced Sensor-wheel with Pressure and Light detection) is developed so as to solve the above mentioned difficulties (Fig. 1). This sensor wheel can measure the mechanical information between the wheel and soil by pressure and light sensors installed on its surface. The system overview of the ASPL is described in Section 2, along with its sensing principle. Experimental tests using the ASPL performed with the single wheel test bed is presented in Section 3. Section 4 discusses several important issues that had not been addressed in the classical wheel model. The conclusions about this study and the future application of the ASPL are summarized in Section 5.

2 Development of ASPL

The detail of the ASPL are described in this section. The ASPL enables to clarify the relationship between the driving characteristics such as a pressure distribution and surface boundary line.

2.1 System overview of ASPL

The breadth and radius of the ASPL are 122 mm and 100 mm. The weight is 2.5 kg. The ASPL is composed of the power supply module, the control module, and the sensor module. The power supply module has a small rechargeable battery (7.4V, 1000mAh) and DCDC converters. The microcontroller board (Arduino mega 2560) and the wireless communication device (XBee ZB PCB Type, frequency 2.4 GHz) are installed on the control module. Also, the sensor module includes pressure sensors, light sensors, and amplifiers. The ASPL contains all of these modules inside and forms self-sustained in-wheel system, enabling an online measurement of wheel driving characteristics. The ASPL sends all of sensing data including pressure, light, and wheel rotation angle to a data logger (laptop PC) used for the wheel experiment, via the XBee. This wireless communication between the ASPL effectively facilitates the data handling in the experiment.

2.2 Detail of sensing principle

The ASPL installs pressure sensors and light sensors on its wheel surface (Fig. 2). Each pressure and light sensors are arranged in the same rotational phase. The sensing area of the ASPL covers 109 degree on the wheel surface. It has 8 sensors each. The interval between the sensors is 4.2 degrees, which becomes the angular resolution. Each sensor channel (the set of pressure and light sensor) is located in the half-phase. Then, when the ASPL rotates, the sensors can continuously measure the characteristics such as pressure distributions or wheel-soil contact angle by contacting with the soil.

In this study, the sensors should be thin and small enough not to generate the additional resistance force. Therefore, the thin pressure sensor Flexiforce (AirBrown Corp.) have been chosen. Its thickness, sensing area, and maximum load are 0.189 mm, ϕ9.5 mm, and 4.4 N respectively. The pressure sensor read-outs the voltage proportional to the force applied to the sensing area. Each pressure sensor has been precisely calibrated with a digital force gage, being its linearity less than $\pm 5\%$.

The light sensors are used to detect the wheel contact angles. The light sensor can geometrically determine the wheel-soil contact angle. The sensor provides “dark” for the wheel subsurface and “bright” as its wheel surface does not touch the ground. The light sensor used here is photoresister VT935A, having the size of 1.8 mm thickness and 4.9×4.2 mm sensing area.

The pressure sensor and light sensor data are correlated with the wheel rotation angle measured by the wheel encoder, with a sampling time 100 ms. Therefore, the pressure distribution and contact angles around the wheel surface can be estimated.

3 Single wheel experiment using ASPL

In this section, experimental studies related to the measurement of the wheel driving characteristics using the ASPL.

3.1 Experimental conditions

The experiment has been performed with a single wheel test bed. The test bed shown in Fig. 3 has dimensions of 1300×600 mm and a height of 450 mm. The wheel can move horizontally and vertically with the slide-guide installed on the test bed. A motor controller

(Overview of the single wheel test bed)

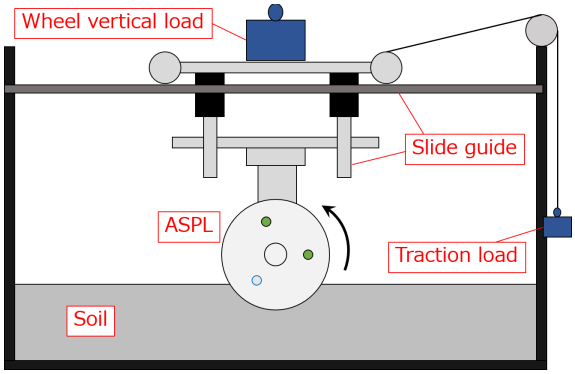

(Schematic view of the single wheel test bed)

Figure 3. Single wheel test bed

with motor driver performs a PID feedback control for the wheel rotation in order to maintain a constant velocity of 10 deg/sec. The translational velocity and the actual wheel sinkage are obtained by the motion capture system prepared at the outside of the test bed. The rotation angle is measured by the encoder of the wheel motor.

In this study, wheel driving characteristics has been measured under the four sets of slip ratio (0.15, 0.3, 0.65, and 0.88). Each slip condition was tested in three times. The slip ratio was regulated by adjusting the traction load connected to the slide guide. Each value of slip ratios had been correlated with corresponding traction loads in advance as shown in Table. 1. The test bed is full of the silica sand No.5. The average particle diameter is 0.51 mm and the density in over-dry condition is 2.61 g/cm^3. The wheel load is 7 kg, allowing the sensing area to contact.

3.2 Evaluation methods for wheel driving

On the loose soil, slip is often observed between the rotating wheel and the sand. It has a great influence upon the behavior or traversability of the rover. Therefore, the slip ratio s is generally used as a metric which expresses the wheel velocity different relative to the wheel rotation. It is defined as this follows.

$$s = \frac{r\omega - v_x}{r\omega} \tag{1}$$

In this equation, v_x and ω are the translational velocity of the rover and the angular velocity of the wheel, respectively.

It is necessary to know the value of the contact angle that is the information how the wheel contact with the soil, in order to calculate the whole force generated under the wheel and to geometrically measure the sinkage.

When a wheel begins to rotate, the sinkage varies depending on the value of slip ratio and then it becomes stable in a position where the normal force from the ground and the wheel load is balanced. Here as shown in Fig. 4, θ_f and θ_r are the angles that are defined as the front or rear contact area between the wheel and soil. In the classical wheel model, these values are defined with the sinkage h of the wheel as follows.

$$\theta_f = \cos^{-1}(1 - h/r) \tag{2}$$
$$\theta_r = \cos^{-1}(1 - \kappa h/r) \tag{3}$$

In especially, κ is a soil reboarding parameter. Because of these equations, the wheel sinkage is also defined as follows.

$$h = r(1 - \cos\theta_f) \tag{4}$$

Consequently, this study wheel focuses on the pressure distribution, contact angle, and wheel sinkage in the various cases of slip ratio to evaluate the interaction between the wheel and soil. Especially, the wheel sinkage is two types: the true sinkage and the measured one. The true sinkage is obtained from the motion capture system outside of the wheel whereas the measured one is determined by the light sensors installed on the ASPL

Table 1. Correspondence of slip ratio and load

slip ratio	load [kg]
0.15	0
0.30	0.10
0.65	0.20
0.88	0.35

3.3 Experimental results

Fig. 5 shows experimental results of the pressure distribution. The plot of this figure expresses the value of pressure sensor while the corresponding light sensor arranged in the same rotational phase detects the subsurface.

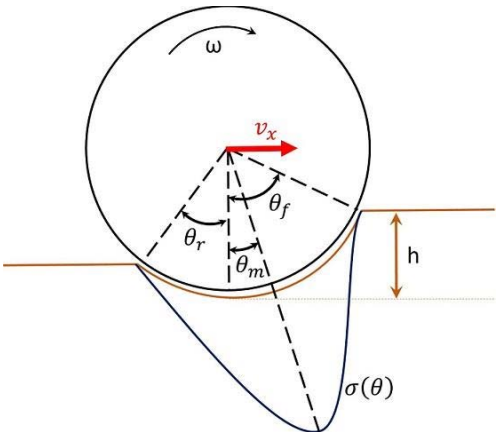

Figure 4. Normal pressure distribution model

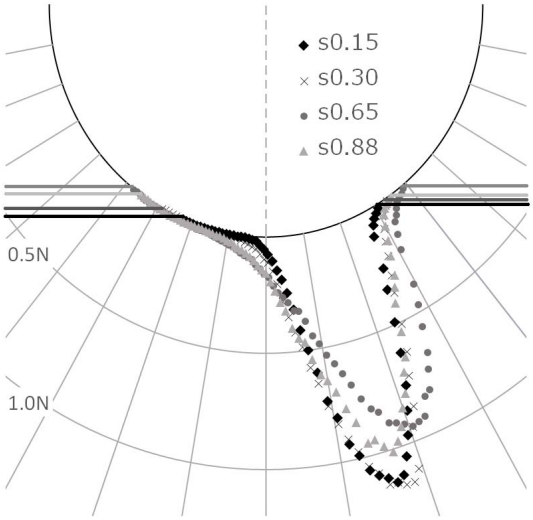

Figure 5. Pressure distribution with regard to varied slip ratio

In this figure, the pressure distribution under four types of slip ratio are drawn in the polar coordinate system. The value plotted is an average value among measured three or more test runs. Fig. 5 clearly shows the shape of pressure distributions, the value of contact angle, and the position of the surface boundary line in each slip ratio. This result indicates that the mechanical relationship of the wheel driving characteristics on loose soil more accurately, also that the light sensor is useful for detecting the contact area, in particular the region where the pressure sensor cannot measure.

Using Equation 4 with the obtained information, the true and measured value of the sinkage and the contact angles (entry angle and exit angle) can be summarized. The relationship of the slip ratio and the sinkage is shown in Fig. 6, and that of the slip ratio and contact angles is shown in Fig. 7. Detailed discussion is described in the following section.

4 Discussion on the experimental result

4.1 Wheel pressure distribution

As shown in the Fig. 5, pressure distributions are similar to each other at the point of its shape, therefore it can be said the ASPL measures the wheel-soil interaction in high repeatability. This result also shows that the peak value of the distributions tends to decrease as the slip ratio increases while the contact patch tends to be large. In general, the wheel translational velocity is getting smaller when the slip ratio becomes large, which leads to the wheel digging the soil surface. Then, the contact patch between the wheel and soil becomes large, resulting in wider pressure distribution like this result.

Also, in Fig. 5, it can be seen the surface boundary line at the both sides of the distribution. The boundary is the point where the light sensor begins or finishes the surface detection. Based on the classical wheel model, the both ends of the pressure distribution is located at the same place where the wheel-soil surface boundary is observed. However, the pressure distribution measured by the ASPL is smaller than the contact area between the wheel and soil. This is because there can be the area where the pressure magnitude from the soil is less than the sensitivity of the pressure sensor. Therefore, the relationship between the pressure distribution and the surface boundary line should be considered independently.

4.2 Wheel sinkage

Fig. 6 shows the relationship between the slip ratio in regard to the true or measured wheel sinkage. The graph shape of the true value and that of the measured value are similar, but some gaps between them are seen. This is due to the fact that the soil in front of the wheel contact remarkably collapses (Fig. 8 and Fig. 9). This phenomenon of the collapse has not been considered carefully in the classical wheel-soil model. In addition, the gap is becomes larger as the value of slip ratio increases. When the slip ratio is small, the wheel can smoothly run with small wheel sinkage and the soil collapse almost does not appear. In contrast, however, the soil collapse has great influence on the large slip ratio since the soil transport effect, which means the soil transportation from the wheel front to the rear. This is the reason why the gap between the true sinkage and the measured one has been observed. It can be also said that another factor of the gap in the each slip ratio may be due to the sampling error shown in the Fig. 9. This is because of the sampling time of 100 ms

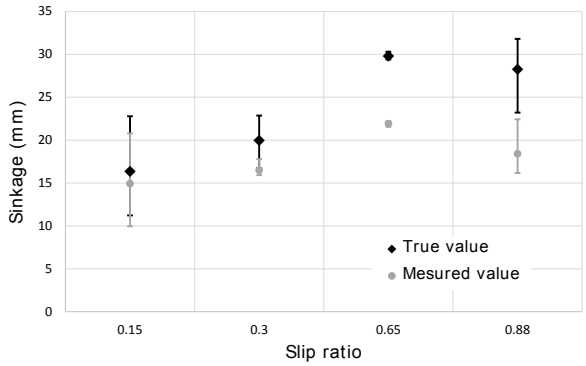

Figure 6. Wheel sinkage evaluation: measured value by ASPL and true value from the motion capture

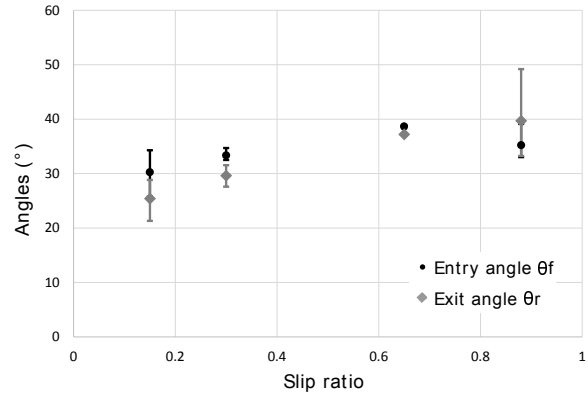

Figure 7. Wheel contact angle evaluation

and wheel rotation velocity of 10 deg/sec.

The wheel sinkage increases as the slip rotation increasing. However, from 0.65 to 0.88, the wheel sinkage decreases. This may be deduced that the wheel-soil interaction changes in that region. Further discussion is described in the following subsection.

4.3 Wheel contact angle

In Fig. 7, the value of θ_f and θ_r tend to increase as the slip ratio. According to Fig. 5, if the slip ratio gets larger, the wheel-soil contact area becomes wider. However, although the angle of θ_f is larger than that of θ_r before slip ratio of 0.65, it becomes smaller in the slip ratio of 0.88. This result is rephrased that the surface boundary line in front of the wheel is higher than that of the rear before the slip ratio of 0.65, but the relation of θ_f and θ_r reverses after that. This result can be explained by the soil transport effect at the wheel-soil interaction as shown in Fig. 10. When the slip ratio is small, the soil bulldozing effect, which means the wheel pushing soil forward, has more influence than the soil transport effect. This interaction makes the angle of θ_f larger than θ_r. In contrast, at the large slip ratio, the soil transport effect has more influence, getting the value of θ_r larger than that of θ_f. As a result, the experimental data provided by the ASPL confirmed that the wheel-soil interaction possesses a slippage-dependent mechanism: the soil bulldozing is a dominant interaction in small wheel slip whereas the soil transportation from the front to the rear can be seen in large wheel slip.

Figure 8. Snapshot view of the soil collapse phenomenon in front of the wheel

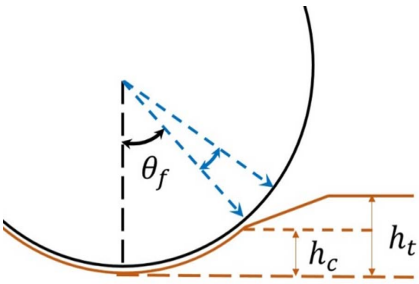

(Schematic view of collapse phenomenon)

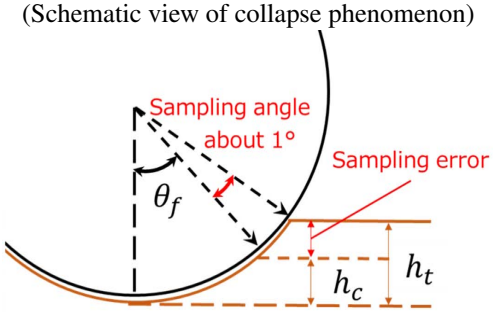

(Schematic view of sampling error)

Figure 9. Reasons for sinkage gap

It should be noted that the ASPL developed in this work has revealed the following physical characteristics: (1) the wheel pressure distribution does not start/end at the edges of the wheel-soil boundary line; (2) the soil collapse in front region of the wheel may be observed in large wheel slip; and (3) the wheel-soil interaction mechanism dynamically changes from the bulldozing in small wheel slip to the transportation in large wheel slip.

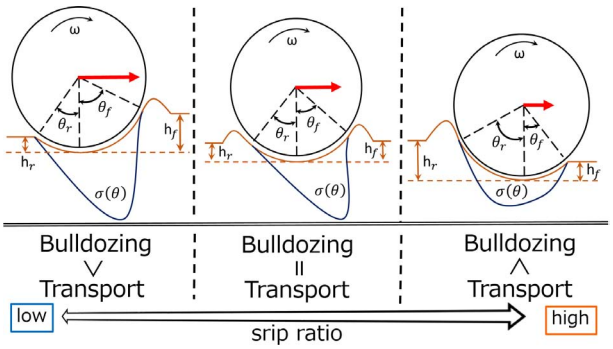

Figure 10. Schematic view of wheel-soil interaction

5 Conclusion

In this study, the in-wheel sensor system called the ASPL has been developed, which can accurately measure the wheel driving characteristics. The experiment using the ASPL has found the following points which have not been well addressed in the classical model: (1) the pressure distribution was formed in the smaller area than the actual contact surface. This result indicates that the pressure distribution should be evaluated separately from the surface boundary line: (2) the gaps between the true wheel sinkage and the measured wheel sinkage was found. The true value was obtained from the motion capture system and the measured one was obtained from the light sensors installed on the ASPL. This gap has got larger as the slip ratio increases owing to the soil collapse in front of the wheel, which was caused by the transport effect. The result also showed the wheel-soil interaction dynamically changes between the slip ratios of 0.65 and 0.88: and (3) according to the experimental result of the contact angle, the entry angle is larger than the exit angle before the slip ratio of 0.65. However, in the slip ratio of 0.88, the exit angle became larger. In the small slip ratio, the bulldozing effect explicitly works to get the entry angle larger. On the other hand, the soil transport effect gets the exit angle larger in the large slip ratio.

The results obtained from the experiments using the ASPL have shown that the ASPL may contribute to the improvement of the classical wheel-soil interaction model. Additional experiment with the particle image velocimetry (PIV) can reveal a detailed pressure distribution process along with the wheel rotation and then will accurately explain the wheel-soil interaction. A possible future application of the ASPL is a hazard detection such as a critical wheel slips by monitoring the pressure quantity as well as the wheel contact angles. Also, the ASPL will be useful for a terrain classification since terrain stiffness can be estimated based on the driving data from the ASPL.

References

[1] M. G. Bekker, *Off-The-Road Locomotion,* Ann Arbor, MI, USA, The University of Michigan Press, 1960.

[2] J. Y. Wong, *Theory of Ground Vehicles,* John Wiley & Sons, 1978.

[3] D. Gee-Clough, "The Bekker Theory of Rolling Resistance Amended to Take Account of Skid and Deep Sinkage," Journal of Terramechanics, Volume 13, Issue 2, pp. 87-105, 1976.

[4] D. Rubinstein, and R. Hitron, "A Detailed Multibody Model for Dynamic Simulation of Off-road Tracked Vehcles," Journal of Terramechanics, pp. 163-173, 2004.

[5] H. Shiby, K. Iagnemma, and S. Dubowsky, " An Equivalent Soil Mechanics Formulation for Rigid Wheels in Deformable Terrain, with Application to Planetary Exploration Rovers, " Journal of Terramechanics, Volume 42, Issue 1, pp. 1-13, 2005.

[6] R. Bauer, W. Leung, and T. Barfoot "Experimental and Simulation Results of Wheel-Soil Interaction for Planetary Rovers." Proc. of the 2005 IEEE/RSJ Int. Conf. on Intelligent Robots and Systems, pp. 586-591.

[7] G. Ishigami, K. Nagatani, and K. Yoshida, "Terramechanics Based Analysis on Slope Traversability for A Pkanetary Exploration Rover," Proc. of the 25th Int. Symp. on Space Technology and Science, pp. 1025-1030, 2006.

[8] O. Lauro, B. Johann, W. Gary, and K. Robert "Terrain Characterization and Classification with a Mobile Robot." Journal of Field Robotics, Volume 23, Issue 2, pp. 103 - 122, 2005.

[9] K. Iagnemma, S. Kang, and C. Brooks, " Multi-Sensor Terrain Estimation for Planetary Rovers, " Proc. of the 7th International Symposium on Artificial Intelligence, Robotics and Automation in Space, 2003.

[10] K. Nagatani, A. Ikeda, K. Sato, and K. Yoshida, " Accurate Estimation of Drawbar Pull of Wheeled Mobile Robots Traversing Sandy Terrain Using Built-in Force Sensor Array Wheel, " Proc. of the 2009 IEEE/RSJ Int. Conf. on Intelligent Robots and Systems, pp. 2373-2378.